Journal of Catalysis **195,** 287–297 (2000)
doi:10.1006/jcat.2000.2994, available online at http://www.idealibrary.com on IDEAL®

Preparation, Characterization, and Performance of FeZSM-5 for the Selective Oxidation of Benzene to Phenol with N_2O

A. Ribera,*,[1] I. W. C. E. Arends,*,[2] S. de Vries,† J. Pérez-Ramírez,‡ and R. A. Sheldon*

*Laboratory for Organic Chemistry and Catalysis, Delft University of Technology, Julianalaan 136, 2628 BL Delft, The Netherlands; †Department of Biotechnology, Delft University of Technology, Julianalaan 67, 2628 BC Delft, The Netherlands; and ‡Section Industrial Catalysis, DelftChemTech, Delft University of Technology, Julianalaan 136, 2628 BL Delft, The Netherlands

Received February 21, 2000; revised May 31, 2000; accepted July 8, 2000

Two isomorphously substituted iron ZSM-5 catalysts with different crystal sizes (2.5 and 0.4 μm) were prepared by hydrothermal synthesis. The samples with a Si/Al ratio of 32 and 34 contained 0.64 and 0.60 wt% of iron, respectively, and were activated by steam at 873 K. The zeolites were characterized by XRD, SEM, TEM, FT-IR, and UV–vis spectroscopy, and EPR. The preparation procedure is an efficient method for obtaining highly crystalline white samples with a high dispersion of iron. Upon calcination and subsequent treatment with steam at 873 K, structural changes occurred. Spectroscopic studies indicated that, during the steaming process, Fe–O–Si bonds were broken and iron migrated toward extraframework positions. EPR revealed that, after the steaming procedure, iron centers with a *g* value of 6 and higher extending to the zero field formed. Both signals disappeared upon reduction, and we suggest that these iron sites are involved in oxidation with N_2O. This zeolite catalyzed the hydroxylation of benzene with nitrous oxide as the oxidant, resulting in high selectivity (>99%) and phenol yields (up to 27%). This is in accordance with previous studies. Experiments with 1,3,5-trimethylbenzene, which is too large to fit inside the pores, demonstrated that the oxidation of benzene to phenol took place within the zeolite pores and not at the external surface.

Key Words: **selective oxidation; nitrous oxide; FeZSM-5; benzene; phenol.**

INTRODUCTION

The selective partial oxidation of hydrocarbons, e.g., the direct conversion of benzene to phenol (1, 2), is still an important objective. Currently, the most widely used industrial route to phenol is the cumene process, in which cumene hydroperoxide undergoes an acid-catalyzed cleavage to yield phenol and acetone. For obvious reasons, a one-step process for the production of phenol, which does not depend on the market price of acetone, is highly preferred. An important source for developing selective catalysts for benzene oxidation are the oxygenases that mediate the selective oxidation of hydrocarbons with O_2 at ambient temperature and pressure. Heme and nonheme iron-containing enzymes, such as cytochrome P450 and methane monooxygenase (MMO), respectively, are two notable representatives of this class of enzymes (3, 4). In most known oxygenases, the iron in the active site is coordinated by a heme protoporphyrin ring; thus, the discovery of MMO, in which a diiron cluster is complexed by amino acid residues (4–6), was remarkable. MMO reductively activates dioxygen for incorporation into a wide variety of hydrocarbon substrates, including alkanes, alkenes, aromatic and aliphatic hydrocarbons, phenols, alcohols, amines, and chlorinated hydrocarbons (4, 7–9).

Significant effort is made to develop biomimetic systems capable of activating oxygen analogous to MMO (10–17). In this context, the synthesis of inorganic biomimetic catalysts, based on high-silica zeolites that contain isolated transition-metal species as active redox sites, is being used to develop new types of catalysts (18, 19). Nanometer-scale engineering of the catalytic function of isolated redox sites in the narrow zeolite channels is of great interest, because confining the redox-active species within the well-defined cavities and/or channels can result in catalysts with unique activity. The inorganic matrix improves the stability of the redox site toward dissociation and/or oxidative destruction just as the protein mantle protects the active site in the enzyme. Moreover, the superstructure of the zeolite can result in an unusual (high-energy) geometry of the metal site, thus enhancing its redox potential. Bioinorganic chemistry describes this as the entactic state (20), which is generally believed to play a major role in determining the activity of metalloenzymes. The term biomimetic thus refers to the catalytic behavior of isolated transition-metal species in a specific environment of the zeolite matrix, which may be similar to the action of enzymes.

In 1988, three groups (21–23) independently discovered that ZSM-5-type zeolites are better catalysts for the direct

[1] Current address: Instituto de Tecnología Química, UPV-CSIC, Universidad Politécnica de Valencia, Avenida de Los Naranjos s/n, 46022, Valencia, Spain.

[2] To whom correspondence should be addressed. Fax: 00 31 152784700. E-mail: I.Arends@tnw.tudelft.nl.

0021-9517/00 $35.00

oxidation of benzene to phenol using nitrous oxide (N_2O) compared to the original V_2O_5/SiO_2 system (24). The latter system required temperatures as high as 823 K when using N_2O to produce phenol with 45% selectivity, while for ZSM-5 catalysts the typical reaction temperature was 623 K and the selectivity for phenol was close to 100%. Panov and co-workers (25–36) continued to develop this system and found a correlation between the amount of iron in the ZSM-5 zeolite and the conversion of benzene to phenol with N_2O. They optimized FeZSM-5 for the benzene-to-phenol conversion and achieved high selectivity (>95%) in all cases.

Panov and co-workers proposed that the active catalyst was a dinuclear iron species, immobilized in the pores of ZSM-5. As such, it resembles the active iron oxidant in MMO, which is capable of transferring one oxygen atom activated on a diiron center to an inactivated C–H bond. Their proposed mechanism is illustrated by reactions [1] and [2]. The authors refer to α-centers, which denote the active sites in the zeolites. The number of active sites is defined as the number of molecules of N_2O that can be decomposed on the surface:

$$N_2O + (\,)_\alpha \rightarrow (O)_\alpha + N_2 \qquad [1]$$

$$C_6H_6 + (O)_\alpha \rightarrow (\,)_\alpha + C_6H_5OH. \qquad [2]$$

The selective oxidative power of these α-sites was demonstrated by the observation that, although they were generated with nitrous oxide at temperatures above 523 K, they could transfer oxygen to benzene or methane at temperatures as low as 243 K (34). This underlines the biomimetic character of these materials. However, the active species is unknown. Some authors claim that either Lewis acidic centers from the extraframework aluminum (37) or extraframework gallium (38) or Brønsted acidic centers from aluminum (39–42) are responsible for the catalytic hydroxylation of benzene to phenol. The fact that commercial ZSM-5 zeolites contain small amounts of iron as impurity must be taken into account.

FeZSM-5 zeolites have been known for over two decades (43, 44) and are of interest for the catalytic reduction of nitrous oxide (45–47) and nitric oxides (48, 49). In most cases, the selective reduction of nitrous oxide is performed with light hydrocarbons (ethane, propane, propene). The presence of hydrocarbons as reducing agents substantially reduces the light-off temperature for the reduction of nitrous oxide and improves the stability of the catalyst in the presence of water vapor compared to the direct N_2O decomposition over FeZSM-5 (45–47). The identity of the active species in this novel process, which may be closely related to benzene-to-phenol oxidation with N_2O, has not yet been established.

The aim of our work is to contribute to the understanding of the structure of the iron site in the steamed, framework-substituted FeZSM-5 catalyst, which can be used for the selective oxidation of benzene to phenol with N_2O. It was reported recently that mild steaming resulted in even better catalytic activity for FeZSM-5 compared to a vacuum treatment at 1173 K (50). We prepared two isomorphously substituted iron zeolites with different crystal sizes. XRD, SEM, TEM, FT-IR, and UV–vis spectroscopy were used to study structural modifications involving iron species induced by calcination and steaming. Furthermore, EPR was used to investigate the iron species in this zeolite.

METHODS

Catalyst Preparation

Two types of iron ZSM-5 zeolites, with Si/Al = 36 and Si/Fe = 152 ratios in the starting synthesis mixture, were prepared by hydrothermal synthesis according to the procedure described below. The difference between these two types of catalysts was the presence (sample FeZSM-5A) or absence (sample FeZSM-5B) of sodium hydroxide in the synthesis gel. In the absence of NaOH, the template concentration was increased to reach the optimum pH. The synthesis mixture contained tetraethylorthosilicate (TEOS, Acros, 98%), tetrapropylammonium hydroxide (Fluka, ~20% in water), iron nitrate nonahydrated (Merck, 99%), aluminum nitrate nonahydrated (Merck, 98.5%), and sodium hydroxide (Aldrich, 97%, only for sample A) in the following nominal molar ratios: $H_2O/Si = 45$, $TPAOH/Si = 0.1–0.3$, $NaOH/Si = 0–0.2$, $Si/Al = 36$, and $Si/Fe = 152$ (see Table 1).

In a typical synthesis, the silica source (TEOS) was added to the organic template (TPAOH) and sodium hydroxide (only in the case of sample A) with stirring. Drops of this solution were added to a mixture of iron and aluminum nitrates dissolved in water. The final solution was transferred to a stainless steel autoclave lined with Teflon and kept in a static air oven at 448 K for 5 days. The crystalline material was separated by filtration and washed with water until the latter was free of nitrate (denoted as catalyst FeZSM-$5A_{as}$ and catalyst FeZSM-$5B_{as}$). These as-synthesized samples were calcined in air at 823 K for 10 h to remove the template. The samples were converted into the H-form by three consecutive exchanges with an ammonium nitrate solution (0.1 M) during the night and subsequent calcination in air at 823 K for 5 h (denoted as samples FeZSM-$5A_c$ and FeZSM-$5B_c$). In the last step, the catalysts were steamed (water partial pressure of 300 mbar and a total flow of 30 ml/min) at high temperature (873 K) for 5 h; they were stored at room temperature in dry air. These samples are denoted as FeZSM-$5A_s$ and FeZSM-$5B_s$, respectively.

Techniques

The chemical analysis was carried out using the ICP-OES technique (Perkin-Elmer Plasma 40 (Si) and Optima

TABLE 1

Molar Ratios of the Gels and Crystalline FeZSM-5 Samples, As Determined by ICP-OES[a]

	Si/Al[b]	Si/Fe[b]	TPAOH/Si[b]	NaOH/Si[b]	Si/Al[c]	Si/Fe[c]	Fe (wt%)[c]
FeZSM-5A_{as}	36	152	0.1	0.2	31.1	126.2	0.59
FeZSM-5A_c	36	152	0.1	0.2	31.6	124.9	0.64
FeZSM-5A_s	36	152	0.1	0.2	31.3	121.7	0.67
FeZSM-5B_{as}	36	152	0.3	—	33.2	131.7	0.54
FeZSM-5B_c	36	152	0.3	—	34.1	130.7	0.60
FeZSM-5B_s	36	152	0.3	—	35.5	128.9	0.61

[a] The error in the values obtained by ICP-OES for the molar ratios amounts to ±2%; (as) as-synthesized, (c) calcined, and (s) steamed samples.
[b] Molar ratios of the gels.
[c] Molar ratios of the crystalline samples.

3000DV (axial)). Powder X-ray diffraction data were collected in the 2θ range of 5 to 50° at a scan rate of 0.5° min^{-1} with a Philips PW 1830/40. For scanning electron microscopy (Philips XL 20), the samples were coated with gold to achieve contrast. For transmission electron microscopy, recorded on a Philips CM 30-T electron microscope with a LaB_6 filament as the source of electrons operated at 300 kV, the samples were mounted on a microgrid carbon polymer supported on a copper grid by placing a few droplets of a suspension of the ground sample in ethanol on the grid, followed by drying under ambient conditions. In order to enhance the visibility of the small particles, the zeolites were amorphized by the electron beam. The Fourier transform infrared (FT-IR) spectra were recorded using a Spectratech diffuse reflectance accessory and a Nicolet Magna 550 Fourier transform spectrometer. The ground, sieved sample (~20 mg) was placed in a holder, which was mounted in a reaction chamber with KBr windows. The calcination step was studied *in situ*. Spectra of FeZSM-5A_{as} were collected in a flow of air (25 ml/min STP) in the range 273 to 823 K (heating rate 10 K/min). The spectrum at 823 K was obtained after 1 h of equilibration. The spectra of FeZSM-5A_s and FeZSM-5B_s were obtained separately in a flow of air at 473 K.

Electronic absorption spectra in the UV and visible range were recorded on a Varian Cary 3 Bio. Diffuse reflectance spectra were recorded in air against $BaSO_4$. EPR samples were studied in dry air or *in situ* by means of a Varian E9 spectrometer at room temperature and at 77 K. Samples were pretreated by calcination at 673 K to remove possible moisture and other contaminants present in the zeolite. To fill the EPR tubes with these samples, a glove box was used to avoid contact with the atmosphere. *In situ* N_2O samples were prepared by letting N_2O (100%) flow at 623 K through a reactor containing the catalyst. After the temperature was reduced to 293 K, the N_2O flow was stopped and the reactor closed to avoid contact with the atmosphere; the reactor was placed into the EPR spectrometer.

Catalytic Oxidation with N_2O

Catalytic tests were carried out in a quartz tube (volume 20 ml, length 58 cm, inner diameter 0.64 mm). The reactor was filled with 0.5 g of the steamed catalyst (pressed into tablets and crushed to 0.50–0.71 mm particle size), and pretreatment was performed *in situ* at 673 K for 1 h in air to remove possible moisture and other contaminants from the zeolite. Benzene was added by means of an evaporator equipped with a thermostat.

The reaction was performed at 623 K and atmospheric pressure. The ratio of benzene : N_2O : nitrogen (carrier gas) was 5 : 20 : 75 (mol%), with the flow corresponding to 0.3 g of benzene per gram of catalyst per hour (1.9 mmol of benzene per hour). The conditions were similar for the oxidation of 1,3,5-trimethylbenzene, cyclohexene, and cyclohexane. Analysis of the reactants and the products was carried out by on-line gas chromatography and FID detection (column: CB-Sil-19, 50 m × 0.53 mm, o.d. = 0.70 mm, d.f. = 1.00 μm, ratio = 132).

RESULTS

Chemical Composition and X-Ray Diffraction

The elemental analysis is given in Table 1. Comparison of the composition of the gels and the crystalline samples indicated that all the iron and aluminum was incorporated into the ZSM-5 crystals. A small part of the silicon was not incorporated. The samples FeZSM-5A_s and FeZSM-5B_s, with a Si/Al ratio of 31 and 35, respectively, typically contained 0.67 and 0.61 wt% of iron, respectively.

Figure 1 shows the XRD patterns of the as-synthesized, calcined, and steamed samples for sample A. There are no significant differences between the XRD patterns of the catalysts FeZSM-5A and FeZSM-5B. All the samples studied showed the characteristic pattern of the MFI structure and the crystallinity of the samples was higher than 95%. Expansion of the unit cell due to the incorporation of iron was not observed because of the low iron content. The

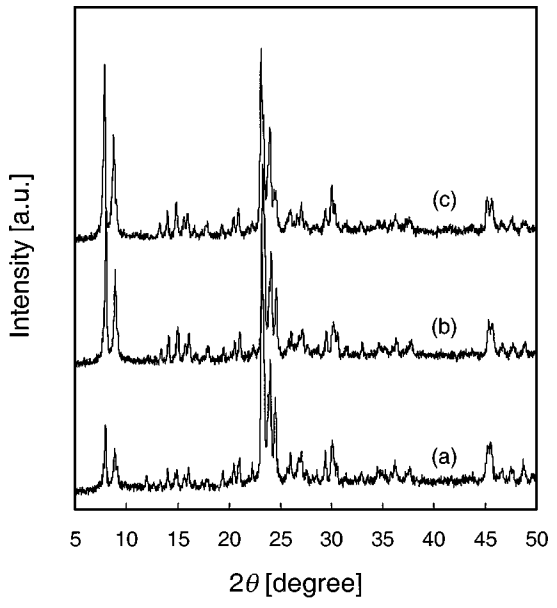

FIG. 1. XRD patterns of (a) FeZSM-5A_{as}, (b) FeZSM-5A_c, and (c) FeZSM-5A_s.

diffractograms did not reveal the reflection of α-Fe_2O_3 (hematite). This indicated that the steam treatment at 873 K did not lead to a significant phase of α-Fe_2O_3. The specific surface areas S_{BET} of both samples were similar, i.e., 363 m^2/g (sample FeZSM-5A_s) and 382 m^2/g (sample FeZSM-5B_s).

Electron Microscopy

Figure 2 shows the scanning electron microscopy (SEM) pictures of samples FeZSM-5A_s and FeZSM-5B_s. No differences in shape or crystallinity were observed for the as-synthesized and calcined samples (not shown). The SEM pictures clearly showed that sample FeZSM-5B_s consisted of smaller crystals (0.4 μm for FeZSM-5B_s versus 2.5 μm for FeZSM-5A_s samples). In other words, at higher template concentration, smaller crystals were obtained. The crystal size distribution of both samples was uniform, and no amorphous matter was detected on the external surface of the zeolite. It was possible to distinguish the crystal intergrowth phenomenon that is typical of ZSM-5 zeolites.

Transmission electron microscopy (TEM) of the steamed samples showed dark spots for FeZSM-5A_s (Fig. 3), which belonged to metal-containing particles. The FeZSM-5B_s sample exhibited a similar pattern (not shown). The size of these particles was around 1 nm. It is assumed that these spots correspond to Fe_2O_3 clusters, which are not identified by XRD. This phenomenon is not uncommon for iron-based zeolites. In fact, we have observed particles of around 10 nm in the case of iron ZSM-5 zeolites, which were synthesized through ion exchange (iron content 0.6 wt%) and then calcined. Thus, in that case, Fe_2O_3 particles were 10 times larger.

Selected area EDX elemental analysis showed a very good distribution of iron throughout the crystals. This, together with the XRD results, indicates that our preparation procedure is an efficient method for obtaining highly dispersed metal-active species, and that the 1-nm Fe_2O_3 clusters represent only a very small fraction of the iron that is actually present in the zeolite. It must be emphasized, however, that any active iron site consisting of single, dinuclear, or even polynuclear species cannot be revealed by this technique.

Infrared Spectroscopy

The infrared spectra for zeolite FeZSM-5A in the hydroxyl stretching (3400 to 3800 cm^{-1}) region are shown in Fig. 4. Spectra for zeolite FeZSM-5B are similar (not shown). The thermal treatment of as-synthesized zeolite FeZSM-5A_{as} was followed *in situ* (spectra a, b, and c). Spectrum d was obtained after proton exchange and steam treatment (see methods section). Complete template removal upon calcination was followed by the disappearance of the characteristic bands in the 2800 to 3000 cm^{-1} region (not shown).

The spectra of the samples exhibited the expected bands in the OH stretching vibration region. The spectrum (Fig. 4a) of the as-synthesized zeolite was dominated by the presence of water. A clear spectrum, expected for the nonacidic zeolite, was observed upon heating to 473 K in air (Fig. 4b). The band around 3740 cm^{-1} is attributed to stretching vibrations of isolated Si–OH groups (51). This vibration was very general and occurred in all samples. The spectrum, observed upon calcination (Fig. 4c), was dominated by a broad absorption ranging from 3400 to 3700 cm^{-1}. This might be due to residual water in the zeolite (as in spectrum a). However, even *in situ* heating of the sample, followed by the recording of the spectrum at 823 K, could not exclude this bulk adsorption. Analogous to the literature (52), this absorption probably corresponds to hydrogen-bonded silanols, which may be located in nests.

Furthermore, a strong, rather broad band at around 3600 cm^{-1}, corresponding to bridging Si(OH)Al groups, appeared (Fig. 4c). The signal for acidic bridging OH groups in aluminum-containing zeolites is usually observed at 3610 cm^{-1} and is characteristic of strong Brønsted acid sites in zeolites (53). The current sample corresponded to the sodium-doped FeZSM-5, which was not yet converted into the H-form and, therefore, displayed limited acid strength. The small number of Brønsted sites together with the high background absorption of hydrogen-bonded silanols probably caused the rather heterogeneous shape of the signal. After the heat treatment, the band near 3740 cm^{-1} shifted to 3720 cm^{-1}. The latter band was previously assigned to terminal silanol groups. It is generally accepted that, while isolated silanols on external surfaces give a narrow band at 3750 cm^{-1}, terminal groups of a

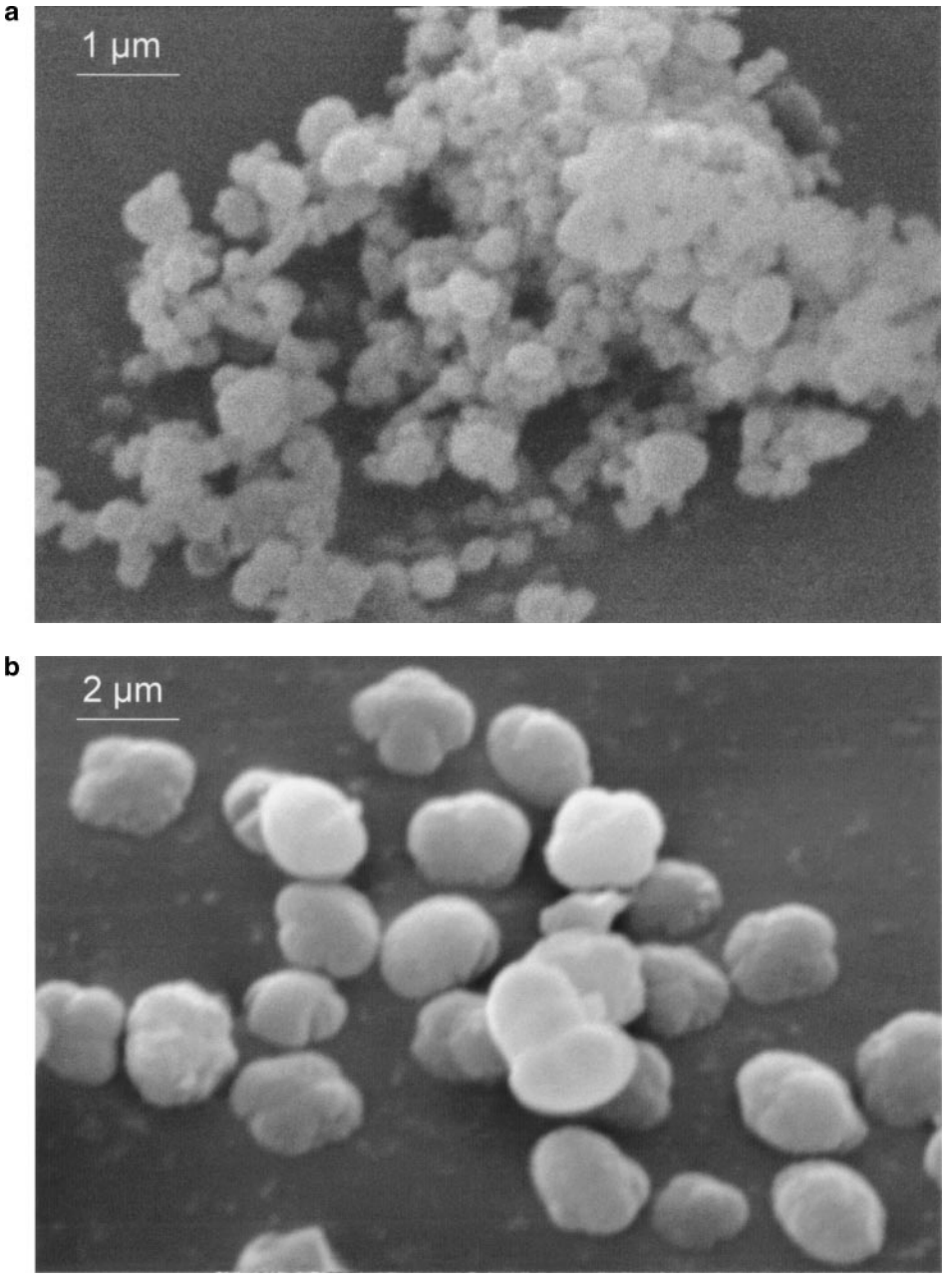

FIG. 2. Electron micrographs (SEM): (a, top) FeZSM-5A_s and (b, bottom) FeZSM-5B_s.

hydrogen-bonded chain absorb at slightly lower wavenumbers. Terminal silanol groups can be formed upon dealumination (52, 54) or when iron is removed from the lattice (55, 56).

After proton exchange and steam treatment at 873 K (Fig. 4d), a number of smaller bands appeared. Particularly visible was the band at 3670 cm^{-1}. This band is usually assigned to extraframework aluminum species (51). For iron silicates, the ν(OH) band for the acidic bridging OH was observed at 3630 cm^{-1} (55, 57). In our study, weak absorption was detected at 3630 cm^{-1} for sample FeZSM-5A_s, but this was largely overshadowed by the bands around 3600 cm^{-1}. From the spectrum, it was impossible to estimate the number of Si(OH)Fe groups. Compared to spectrum c, the broad absorption band from 3700 to 3400 cm^{-1} decreased in spectrum d, while the band assigned to the silanol groups shifted back to 3740 cm^{-1}. This indicated that steaming induces dehydroxylation accompanied by "closure" of the nests.

Ultraviolet–Visible Spectroscopy

The UV–visible reflectance spectra of as-synthesized, calcined, and steamed samples of sample A are presented

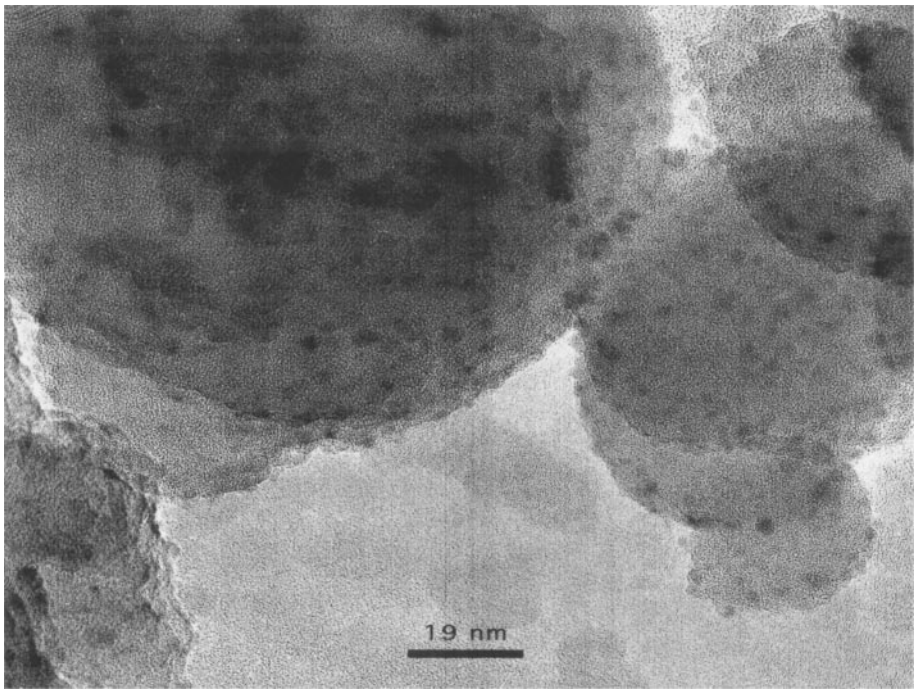

FIG. 3. Electron micrograph (TEM) picture of FeZSM-5A$_s$.

in Fig. 5. Similar spectra were obtained for sample B (not shown). The as-synthesized and calcined samples were white, whereas the steamed samples were tan. All spectra were dominated by a strong absorption in the 200- to 350-nm interval (two maxima are clearly distinguished), due to the metal–oxygen charge transfer.

In accordance with the molecular orbital diagram of Tippins (58), two bands were observed at 212 and 234 nm in the as-synthesized and calcined samples. These bands can be assigned to the $t_1 \rightarrow t_2$ and $t_1 \rightarrow e$ transitions. These strong bands appeared in the same energy range for both the octahedral and the tetrahedral complexes. Thus, the mere presence of these two bands cannot be regarded as a conclusive proof of the tetrahedral coordination state of iron.

The calcination step to remove the template and the steaming treatment resulted in clear modifications of the UV–visible spectra: (i) broadening of the charge transfer

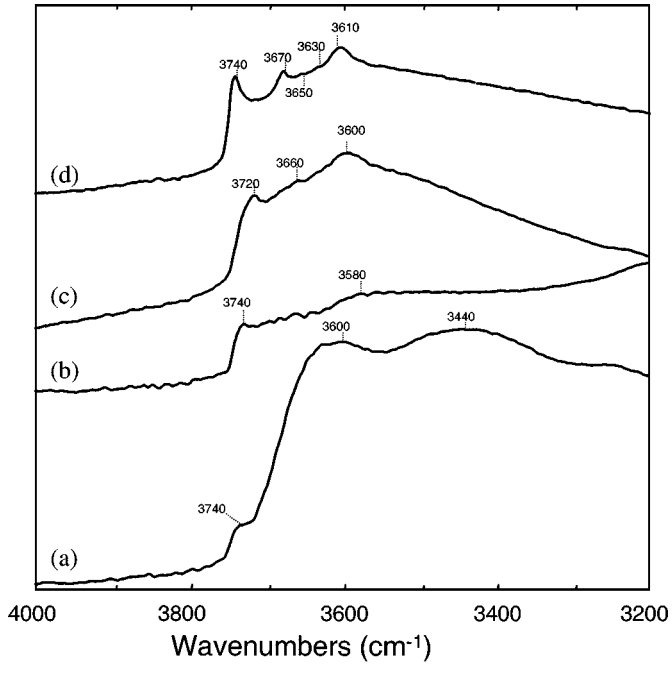

FIG. 4. Infrared spectra of FeZSM-5A in air flow after different treatments: (a) FeZSM-5A$_{as}$ at 293 K; (b) FeZSM-5A$_{as}$ after *in situ* heating to 473 K; (c) FeZSM-5A$_{as}$ after *in situ* calcination at 823 K; (d) FeZSM-5A$_s$ at 473 K.

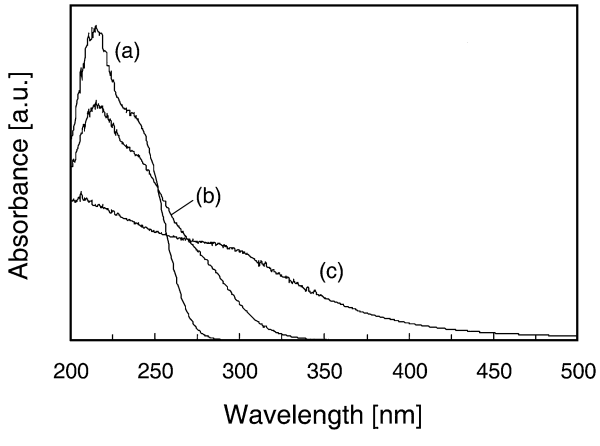

FIG. 5. Diffuse reflectance, UV–vis spectra of (a) FeZSM-5A$_{as}$, (b) FeZSM-5A$_c$, and (c) FeZSM-5A$_s$. Spectra recorded in air.

bands, (ii) a shift toward higher wavelengths, (iii) an increase in absorbance in the high-wavelength tail, and (iv) a decrease in the number of the bands centered at 212 and 234 nm. The disappearance of the peak centered at 212 nm was accompanied by absorption around 280 nm. The peak at 280 nm corresponded to the absorption of iron in octahedral complexes (56). This indicated that iron might be present as isolated or clustered iron oxide species (59, 60), i.e., oxidic microaggregates. This is in agreement with our TEM results (see above).

Electron Paramagnetic Resonance

X-band EPR spectra were recorded for as-synthesized, calcined, and steamed samples, respectively. Furthermore, spectra were acquired *in situ* for steamed samples, which were activated with N_2O at 623 K and then cooled *in situ*. Samples FeZSM-5A and FeZSM-5B displayed the same spectra with the exception of minor differences in the relative intensity. Figure 6 shows the spectra for sample A. Signals appeared at $g = 2.0$ and $g = 4.3$ for all of our samples. For the as-synthesized sample, the spectrum displayed a weak signal at $g = 2.2$.

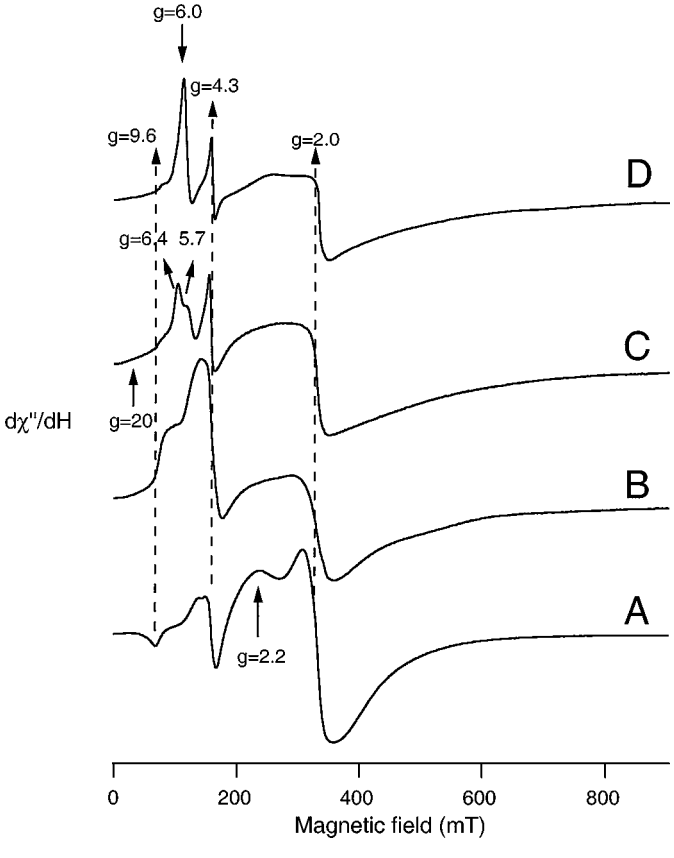

FIG. 6. EPR spectra, recorded at 298 K in dry air, of (A) FeZSM-$5A_{as}$, (B) FeZSM-$5A_c$, (C) FeZSM-$5A_s$, and (D) FeZSM-$5A_s$ *in situ* activated with N_2O.

These signals are typical of Fe in zeolites, and are in accordance with the literature (61). The appearance of a signal at $g = 4.3$ was often regarded as evidence of framework substitution in zeolites and AlPOs, while the line at $g = 2.0$ was always attributed to extraframework Fe(III) at cationic positions (62–67). The $g = 2.2$ signal was commonly assigned to iron in interstitial oxide and hydroxide phases (68). However, Wichterlová and Jiru (69) and other authors (61, 70) pointed out that the signal at $g = 4.3$ may be due, at least in part, to the extraframework Fe(III) species at cationic sites. Vedrine *et al.* (71) were the first to report that not only a signal at $g = 4.3$, but also at $g = 2.0$, might be indicative of framework Fe. We thus conclude that the assignment of the structure of the iron species in zeolites is by no means unambiguous.

Calcination of the catalysts caused some changes in the EPR spectra. As can be seen from Fig. 6B, the signals are now at $g = 2.0$ and $g = 4.3$, accompanied by the signal at $g = 9.6$. The latter signal is due to transitions in the lower and upper doublets of rhombic ($E > D$) high-spin Fe^{3+}, in which E is the rhombic and D the axial zero-field splitting parameter. The same species yielded the (almost) isotropic signal at $g = 4.3$, originating from the transition in the middle doublet (72). After steam treatment of the catalysts at 873 K (Fig. 6C), two new signals appeared at $g = 6.0$ and at low field around $g = 20$ (see below). Furthermore, the intensity of the signal at $g = 4.3$ decreased. The $g = 6.0$ signal is ascribed to a high-spin penta- or hexacoordinated iron (III) in axial distorted symmetry and has been observed before (70, 73, 74).

The signal near zero field was broad and was difficult to recognize from the spectra. The proof of the presence of a signal near zero field was given by the experiment at 77 K. Figure 7 presents spectra that were recorded at 77 K for sample FeZSM-$5A_s$ before and after the addition of β-mercaptoethanol. At 77 K, the $g = 6$ signal split into two signals with $g = 6.4$ and $g = 5.7$. Addition of β-mercaptoethanol resulted in the disappearance of the $g = 6.4/5.7$ signals and of the broad absorbance indicated by $g = 20$. This suggests that both signals correspond to redox-active species. The fact that the signal at low field disappeared upon reduction indicated that this is due to Fe^{3+} and not to Fe^{2+}.

The maximum g value for a single Fe^{3+} ion is $g = 9.5$–10 for high-spin ($S = \frac{5}{2}$) Fe^{3+} (75, 76). This signal was in fact observed (see $g = 9.6$ signal in Figs. 6 and 7). No signals due to mixed-valence Fe^{2+}–Fe^{3+} clusters were observed (expected at g values of 1.6 to 2.0). By inference, signals with g values above $g = 10$ cannot be due to isolated Fe^{3+} or Fe^{2+} centers and must be due to clusters consisting of two or more Fe^{3+} ions (75, 76). The smallest cluster is a binuclear center. The total spin at such a binuclear Fe center could be $S = 5$ (two ferromagnetically coupled high-spin ($S = \frac{5}{2}$) Fe^{3+}, yielding a species with a signal around $g = 20$. Since the observed resonance was broad and extends to zero field, such a

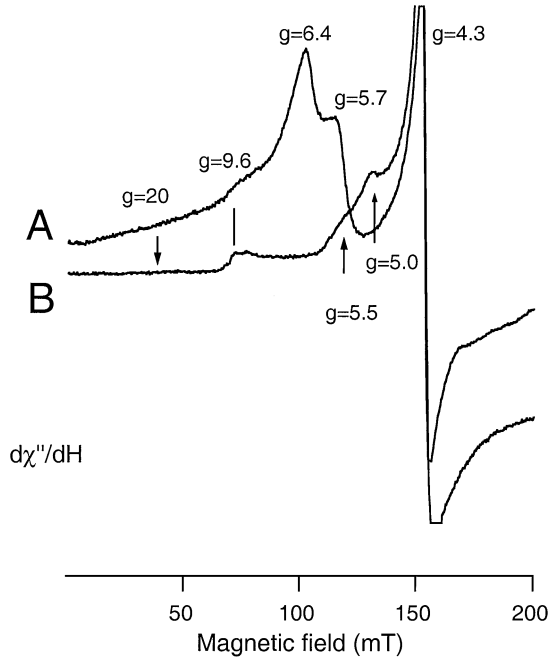

FIG. 7. EPR spectra recorded at 77 K of steamed FeZSM-5A_s, (A) before and (B) after addition of β-mercaptoethanol.

binuclear species might be heterogeneous, occupying different positions in the framework. This resonance may also originate from clusters with a nuclearity above two.

Furthermore, upon reduction, new signals appeared around $g = 5.0$ and $g = 5.5$ (Fig. 7), while these signals might be due to a modified form of the tetrahedral framework iron ($g = 4.3$), the $g = 5.0$ signal might also be due to a transition in the $|\pm\frac{3}{2}\rangle$ doublet of an $S = \frac{7}{2}$ system.

In situ treatment of the steamed samples with N_2O at 623 K affected the relative intensity of the signals but did not yield any new signals (Fig. 6D). The intensity of the $g = 6$ signal increased with respect to the $g = 4.3$ signal. When FeZSM-5A_s was subjected to water vapor or ammonia vapor the $g = 6.4/5.7$ signals disappeared. This was observed before (73). The interaction of coordinatively unsaturated and/or distorted Fe(III) with these strong ligands apparently resulted in a decrease in field symmetry, i.e., a higher E/D ratio, and caused a shift in the EPR signals to lower g values, i.e., $g = 4.3$.

Catalytic Activity

The results obtained for the oxidation of benzene with nitrous oxide over the FeZSM-5 samples FeZSM-5A_s and FeZSM-5B_s at 623 K are presented in Fig. 8. On the basis of GC analysis, phenol was produced with 100% selectivity. In the absence of N_2O, using a stream of benzene diluted with nitrogen, benzene was not consumed (not shown). The activity was similar to that reported previously (50), i.e., an initial conversion of 35% declining to 15.5% after 3 h (unspecified conditions). Deactivation in this process was ascribed to coke deposition (27).

Our study showed a loss of catalytic activity with time on stream (Fig. 8). The two catalyst samples A and B displayed different profiles. For sample FeZSM-5A_s the initial yield after 5-min time on stream was 1.03 mmol of phenol/h · g_{cat}, which corresponds to a 27% yield. The activity decreased to 16% yield after 3 h. In contrast, catalyst FeZSM-5B_s, with a smaller crystal size, showed a lower initial yield of 18% (0.692 mmol of phenol/h · g_{cat}) after 5-min time on stream. However, a slower deactivation was noted: the yield of phenol after 3-h time on stream was still 20%. Selectivity in all cases was close to 100% and remained constant with time on stream. This indicated that there were no changes in the mechanism of the reaction during deactivation and that the decrease in activity was probably due only to the blocking of the channels and, thus, to a decrease in the number of active sites. The difference in the deactivation profiles of our two samples can be explained by the fact that, in the case of smaller crystals as well as in the case of catalyst FeZSM-5B_s, deactivation is likely to be a slower process.

We also studied benzene oxidation with nitrous oxide, under the same conditions at 623 K, using a commercial acidic ZSM-5 with a Si/Al ratio of 36 (Fig. 8). A maximum of 1% phenol was formed, which was more than a factor of 10 below the levels of conversion obtained with the iron-containing ZSM-5 samples. This observation is in accordance with other studies, which reported benzene-to-phenol conversion with nitrous oxide for ZSM-5 zeolites (see above). Admittedly, this zeolite sample was not steamed, which might have increased conversion (37). However, the discrepancy between the results for the "noniron" zeolite and our prepared FeZSM-5 samples is such as to strongly suggest that the presence of iron is essential.

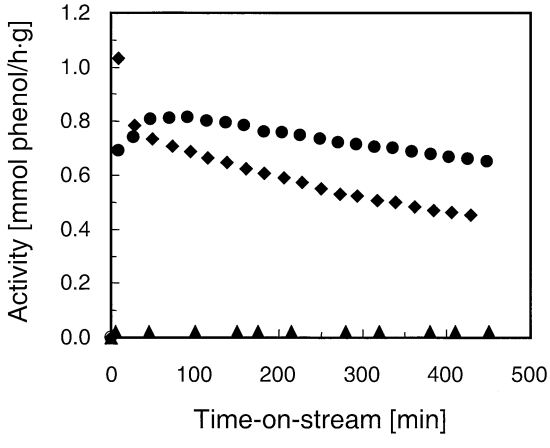

FIG. 8. Conversion of benzene to phenol over FeZSM-5A_s (■), FeZSM-5B_s (◆), and commercial ZSM-5 (Si/Al = 36) (▲) versus time on stream at 623 K.

The oxidation of 1,3,5-trimethylbenzene (TMB) over FeZSM-5A_s was also investigated. The kinetic diameter of TMB is around 8 Å, which makes it too large to fit into the channels of ZSM-5. When applying TMB as a substrate in the reaction under identical experimental conditions, no products were observed. This indicated that the active sites for the oxidation with nitrous oxide were located inside the pores, and negligible activity was exhibited by the outer surface.

We attempted to oxidize cyclohexene and cyclohexane with N_2O over the Fe-ZSM-5 catalyst in the range 523 to 623 K. For these substrates, <3% conversion was obtained, and numerous products were observed by GC (C6 and lower). Selective oxidation—as for benzene—did not seem to occur.

DISCUSSION

We investigated the result of steam treatment on ZSM-5 zeolite with a Si/Al ratio of 36 (in the starting synthesis gel) containing iron at framework positions. It was shown that steaming of the zeolites was necessary to increase the activity of the catalyst (benzene-to-phenol oxidation with nitrous oxide) to levels and selectivities that are of interest to industry (50). Steam treatment is the usual method for modifying zeolites by breaking the Si–O–T bonds (where T = Al/Fe).

Studies have been made of the thermal activation of ferrisilicalites, also under high-temperature (>773 K) conditions (55, 56). The IR spectra gave very valuable information: the bridging hydroxyl Si(OH)Fe group at 3630 cm^{-1} was monitored, and these bridging hydroxyls—and thus iron from the framework—disappeared upon thermal treatment at 973 K. In contrast, in our study of aluminum-containing framework-substituted FeZSM-5, the band at 3630 cm^{-1} for bridging Si(OH)Fe was weak and not very clear, being overshadowed by the broad signal of Si(OH)Al around 3610 cm^{-1}. IR spectra enabled us to monitor the process of dealumination by following the changes in the bridging hydroxyl Si(OH)Al band and the formation of extraframework aluminum species (absorption band at 3670 cm^{-1}). Upon steaming, the terminal Si–OH groups (absorption band at 3720 cm^{-1}), which had appeared after calcination, disappeared. This is consistent with "closure" of the silanol nests, as observed by a considerable decrease in the broad adsorption ranging from 3400 to 3700 cm^{-1} (55, 56).

The UV spectra indicated that iron moved toward octahedral positions, which would correspond to the formation of extraframework species such as Fe_2O_3 clusters. The formation of extraframework iron oxide and/or aluminum oxide species is a process that is commonly observed for different zeolites upon calcination. Other researchers observed iron oxide clusters in FeZSM-5 zeolites that were prepared according to different methods. Fejes *et al.* (68) observed the production of amorphous Fe_2O_3 with a very high molecular dispersity for isomorphously substituted FeZSM-5 zeolites (Si/Fe = 15) after careful calcination. They too could not observe any reflection for α-Fe_2O_3 in the XRD. They estimated, from their Mössbauer results, that these Fe_2O_3 clusters were smaller than 3 nm. Joyner and Stockenhuber (77) published EXAFS results for FeZSM-5 zeolites prepared by aqueous exchange and calcination in air at 773 K. They found small oxygen-containing nanoclusters within the zeolite matrix, with an average composition of Fe_4O_4. We propose that the particles that we observed by TEM are similar to those microoxidic clusters.

Infrared studies (55, 56) of ferrisilicalites showed that calcination up to 973 K caused migration of iron from framework to extraframework positions as well as the elimination of Brønsted acidity. At the same time, water molecules were nucleated from silanol nests. According to the IR and UV studies, we suggest that this process takes place simultaneously for the removal of iron as well as of aluminum from the lattice.

EPR data provided more information about the structure of these extraframework species. While the signals at $g = 2$ and $g = 4.3$ are unspecific, the signal at $g = 6$, corresponding to rhombic high-spin iron, is not usually observed in zeolites. El-Malki *et al.* (73) and Kucherov *et al.* (78) observed this site in FeZSM-5 samples that were prepared by careful sublimation of $FeCl_3$ into the pores of commercial H-ZSM-5. This signal was assigned to very reactive isolated Fe^{3+} species in this less distorted tetrahedral coordination. Disappearance of the signal was observed upon interaction with NO and NO_2 (78).

Recently Volodin *et al.* (74) carried out an *in situ* ESR study of FeZSM-5, which had been prepared through ion exchange followed by thermal activation *in vacuo* at 1073 K. They proposed using the $g = 6$ signal—or rather the disappearance thereof—as a probe for the reactivity of this material with N_2O. In their studies, the appearance and disappearance of the signal was very sensitive to vacuum treatment, and to the presence of water and NO. In our EPR spectra, the $g = 6$ signal appeared after activation of the FeZSM-5 zeolite with steam. The above-mentioned FeZSM-5 zeolites, which contained iron in this high-spin rhombic coordination, had been demonstrated to be excellent catalysts for NO_x reduction and N_2O-mediated oxidation (73, 78). We propose that high-spin rhombic iron can play a role in the activation of N_2O in our system for benzene-to-phenol oxidation.

The signal for Fe^{3+} extending to zero field, which we observed around $g = 20$, had not been reported before. According to EPR theory, this signal should correspond to iron atoms with coupled spin. The resonance is admittedly broad, possibly due to the heterogeneous character of the zeolite framework, and requires further study. EPR studies in the parallel mode should give a better description of the origin of the signal. In principle, this signal may indicate

the presence of active dinuclear iron species, analogous to those found in the MMO nonheme iron-containing enzyme, as has been suggested by Panov and co-workers (see above). For overexchanged iron ZSM-5 catalysts prepared according to the Chen and Sachtler (49) method (Al/Fe ratio = 1, and Si/Al ratio = 17), the presence of binuclear iron oxo/hydroxo complexes was demonstrated by XAFS (79).

The extraframework irons that we identified by UV and TEM, and that were present as well-dispersed microoxidic clusters in octahedral coordination, were probably not the active species we were looking for. EPR indicated a reactive iron site (represented by a signal at $g = 6$) in less distorted tetrahedral coordination.

The nonreactivity of 1,3,5-trimethylbenzene indicated that the active sites for oxidation with nitrous oxide were located inside the pores, and negligible activity was exhibited by the outer surface. This was in accordance with the EDX analysis that showed that iron sites were well distributed throughout the zeolite crystal.

CONCLUSIONS

Starting from a well-defined, framework-incorporated FeZSM-5, our spectroscopic results show that the steaming procedure causes the breaking of the Fe–O–Si bonds and leads to the formation of well-dispersed extraframework iron species. The EPR experiments reveal redox-active iron centers with a g value of 6 and a rather broad adsorption around $g = 20$. We suggest these signals to be important probes for future studies of the reactivity of iron zeolites. The extraframework iron clusters with octahedral symmetry, which are formed upon steam treatment of framework-substituted FeZSM-5, are, very likely, not participating in the reaction.

ACKNOWLEDGMENTS

A.R. acknowledges the Ministerio de Educación y Cultura for a postdoctoral grant, and I.W.C.E.A. gratefully acknowledges a fellowship granted by the Royal Netherlands Academy of Arts and Sciences. We thank Dr. P. Kooijman of the National Centre for High Resolution Electron Microscopy, Delft University of Technology, for performing the TEM study, Dr. A. van der Kraan of the Interfacultary Reactor Institute, Delft University of Technology for conducting the Mössbauer experiments, and Prof. G. I. Panov, Dr. V. I. Sobolev, Dr. J. C. van der Waal, and Dr. G. Clet for valuable discussions.

REFERENCES

1. Sheldon, R. A., and Kochi, J. K., "Metal Catalyzed Oxidations of Organic Compounds." Academic Press, New York, 1981.
2. Fanz, G., and Sheldon, R. A., "Uhlmann's Encyclopedia of Industrial Chemistry," Vol. A18, p. 261. VCH, Weinheim, 1991.
3. Sono, M., Roach, M. P., Coulter, E. D., and Dawson, J. H., *Chem. Rev.* **96**, 2841 (1996).
4. Waller, B. J., and Lipscomb, J. D., *Chem. Rev.* **96**, 2625 (1996).
5. Feig, L., and Lippard, S. J., *Chem. Rev.* **94**, 759 (1994).
6. Rosenzweig, A. C., and Lippard, S. J., *Acc. Chem. Res.* **27**, 229 (1994).
7. Colby, J., Stirling, D. I., and Dalton, H., *Biochem. J.* **165**, 395 (1977).
8. Green, J., and Dalton, H., *J. Biol. Chem.* **264**, 17698 (1989).
9. Fox, B. G., Borneman, J. G., Wackett, L. P., and Lipscomb, J. D., *Biochemistry* **29**, 6419 (1990).
10. "Oxygenases and Model Systems" (T. Funabiki, Ed.). Kluwer, Dordrecht, 1996.
11. Udenfriend, S., Clark, C. T., Axelrod, J., and Brodie, B. D., *J. Biol. Chem.* **208**, 731 (1954).
12. Kitajima, N., Fukui, H., and Moro-oka, Y., *J. Chem. Soc., Chem. Commun.* 485 (1988).
13. Kim, C., Chen, K., Kim, J., and Que, L., *J. Am. Chem. Soc.* **119**, 5964 (1997).
14. Barton, D. H. R., and Doller, D., *Acc. Chem. Res.* **25**, 504 (1992).
15. Barton, D. H. R., and Taylor, D. K., *Pure Appl. Chem.* **68**, 497 (1996).
16. Que, L., and Dong, Y., *Acc. Chem. Res.* **29**, 190 (1996), and references cited therein.
17. Kim, K., and Lippard, S. J., *J. Am. Chem. Soc.* **118**, 4914 (1996).
18. Parton, R. F., Vankelecom, I. F. J., Casselman, M. J. A., Bezoukhanova, C. P., Uytterhoeven, J. B., and Jacobs, P. A., *Nature* **370**, 541 (1994).
19. Arends, I. W. C. E., Sheldon, R. A.,Wallau, M., and Schuchardt, U., *Angew. Chem., Int. Ed. Engl.* **36**, 1144 (1997).
20. Williams, R. J. P., *Eur. J. Biochem.* **234**, 363 (1995).
21. Suzuki, E., Nakashiro, K., and Ono, Y., *Chem. Lett.* 953 (1988).
22. Gubelmann, M., and Tirel, P.-J., Fr. Patent 2.630.735, 1988.
23. Kharitonov, A. S., Alexandrova, T. N., Vostrikova, L. A., Ione, K. G., and Panov, G. I., Russ. Patent 4.445.646, 1988.
24. Iwamoto, M., Hirata, J. I., Matsukami, K., and Kagawa, S., *J. Phys. Chem.* **87**, 903 (1983).
25. Panov, G. I., Sobolev, V. I., and Kharitonov, A. S., *J. Mol. Catal.* **61**, 85 (1990).
26. Panov, G. I., Sheveleva, G. A., Kharitonov, A. S., Rommannikov, V. N., and Vostrikova, L. A., *Appl. Catal. A* **82**, 31 (1992).
27. Panov, G. I., Kharitonov, A. S., and Sobolev, V. I., *Appl. Catal. A* **98**, 1 (1993).
28. Kharitonov, A. S., Sheleva, G. A., Panov, G. I., Sobolev, V. I., Paukshtis, Y. A., and Romannikov, V. N., *Appl. Catal. A* **98**, 33 (1993).
29. Sobolev, V. I., Panov, G. I., Kharotonov, A. S., Romannikov, V. N., Volodin, A. M., and Ione, K. G., *J. Catal.* **139**, 435 (1993).
30. Sobolev, V. I., Dubkov, K. A., Paukshtis, E. A., Pirutko, L. V., Rodkin, M. A., Kharitonov, A. S., and Panov, G. I., *Appl. Catal. A* **141**, 185 (1996).
31. Panov, G. I., Sobolev, V. I., Dubkov, K. A., and Kharitonov, A. S., *Stud. Surf. Sci. Catal.* **101**, 493 (1996).
32. Dubkov, K. A., Sobolev, V. I., Talsi, E. P., Rodkin, M. A., Watkins, N. H., Shteinman, A. A., and Panov, G. I., *J. Mol. Catal. A: Chem.* **123**, 155 (1997).
33. Panov, G. I., Sobolev, V. I., Dubkov, K. A., Parmon, V. N., Ovanesyan, N. S., Shilov, A. E., and Shteinman, A. A., *React. Kinet. Catal. Lett.* **61**, 251 (1997).
34. Dubkov, K. A., Sobolev, V. I., and Panov, G. I., *Kinet. Catal.* **39**, 72 (1998).
35. Panov, G. I., Uriarte, A. K., Rodkin, M. A., and Sobolev, V. I., *Catal. Today* **41**, 365 (1998).
36. Ovanesyan, N. S., Shteinman, A. A., Dubkov, K. A., Sobolev, V. I., and Panov, G. I., *Kinet. Catal.* **39**, 792 (1998).
37. Motz, J. L., Heinichen, H., and Hölderich, W. F., *J. Mol. Catal. A: Chem.* **136**, 175 (1998).
38. Häfele, M., Reitzmann, A., Roppelt, D., and Emig, G., *Appl. Catal. A* **150**, 153 (1997).
39. Ono, Y., Tohmori, K., Suzuki, S., Nakashiro, K., and Suzuki, E., *in* "Heterogeneous Catalysis and Fine Chemicals" (M. Guisnet, J. Barrault, C. Bouchoule, D. Duprez, C. Montassier, and G. Pérot, Eds.). p. 75. Elsevier, Amsterdam, 1988.

40. Gubelmann, M., and Tirel, P.-J., E.P. Patent 341.165 and U.S. Patent 5.001.280, 1989.
41. Burch, R., and Howitt, C., *Appl. Catal. A* **86**, 139 (1992).
42. Burch, R., and Howitt, C., *Appl. Catal. A* **103**, 135 (1993).
43. McNicol, B. D., and Pott, G. T., *J. Catal.* **25**, 223 (1972).
44. Szostak, R., Nair, V., and Thomas, T. L., *J. Chem. Soc., Faraday Trans. 1* **83**, 487 (1987).
45. Kögel, M., Mönnig, R., Schwieger, W., Tissler, A., and Turek, T., *J. Catal.* **182**, 470 (1999).
46. Pophal, C., Yogo, T., Tanabe, K., and Segawa, K., *Catal. Lett.* **44**, 271 (1997).
47. Pérez-Ramírez, J., García-Cortés, J. M., Kapteijn, F., Illán-Gómez, M. J., Ribera, A., Salinas-Martínez de Lecea, C., and Moulijn, J. A., *Appl. Catal.B* **25**, 191 (2000).
48. Feng, X., and Hall, W. K., *J. Catal.* **166**, 368 (1997).
49. Chen, H.-Y., and Sachtler, M. H., *Catal. Today* **42**, 73 (1998).
50. Kharitonov, A. S., Panov, G. I., Sheveleva, G. A., Pirutko, L. V., Voskresenskaya, T. P., and Sobolev, V. I., U.S. Patent 5.672.777, 1996.
51. Fritz, P. O., and Lunsford, J. H., *J. Catal.* **118**, 85 (1989).
52. Zecchina, A., Bordiga, S., Spoto, G., Scarano, D., Petrini, G., Leofanti, G., Padovan, M., and Otero Aréan, C., *J. Chem. Soc., Faraday. Trans.* **88**, 2959 (1992).
53. Aronson, M. T., Gorte, R. J., and Farneth, W. E., *J. Catal.* **105**, 455 (1987).
54. Zecchina, A., Bordiga, S., Spoto, G., Marchese, L., Petrini, G., Leofanti, G., and Padovan, M., *J. Phys. Chem.* **96**, 4985 (1992).
55. Zecchina, A., Geobaldo, F., Lamberti, C., Bordiga, S., Turnes Palomino, G., and Otero Aréan, C., *Catal. Lett.* **42**, 25 (1996).
56. Bordiga, S., Buzzoni, R., Geobaldo, F., Lamberti, C., Giamello, E., Zecchina, A., Leofanti, G., Petrini, G., Tozzola, G., and Vlaic, G., *J. Catal.* **158**, 486 (1996).
57. Chu, C. T.-W., and Chang, C. D., *J. Phys. Chem.* **89**, 1569 (1985).
58. Tippins, H. H., *Phys. Rev. B* **1**, 126 (1970).
59. Lehmann, G., *Z. Phys. Chem. Neue Folge* **72**, 279 (1970).
60. Bongiovanni, R., Pellizzetti, E., Borgarello, E., and Meisel, D., *Chim. L'Ind.* **4**, 261 (1994).
61. Goldfarb, D., Bernardo, M., Strohmaier, K. G., Vaughan, D. E. W., and Thomann, H., *J. Am. Chem. Soc.* **116**, 6344 (1994).
62. Gao, Z., Tian, D., and Zhou, R., *Zeolites* **8**, 453 (1988).
63. Kotasthane, A. N., Shiralkar, V. P., Hegde, S. G., and Kulkarni, S. B., *Zeolites* **6**, 253 (1986).
64. Inui, T., Nagata, H., Takeguchi, T., Iwamoto, S., Matsuda, H., and Inoue, M., *J. Catal.* **139**, 482 (1993).
65. Ratnasami, P., and Kumar, R., *Catal. Today* **9**, 328 (1991).
66. Joshi, P. N., Awate, S. V., and Shiralkar, V. P., *J. Phys. Chem.* **97**, 9749 (1993).
67. Brückner, A., Lohse, U., and Mehner, H., *Microporous Mesoporous Mater.* **20**, 207 (1998).
68. Fejes, P., Nagy, J. B., Lázár, K., and Halász, J., *Appl. Catal. A* **190**, 117 (2000).
69. Wichterlova, B., and Jiru, P., *React. Kinet. Catal. Lett.* **13**, 197 (1980).
70. Kucherov, A. V., and Slinkin, A. A., *Zeolites* **8**, 110 (1988).
71. Lin, D. H., Coudurier, G., and Vedrine, J. C., *Stud. Surf. Sci. Catal.* **49B**, 1423 (1989).
72. Castner, T., Jr., Newell, G. S., Holton, W. C., and Slichter, C. P., *J. Chem. Phys.* **32**, 668 (1960).
73. El-Malki, E.-M., van Santen, R. A., and Sachtler, W. M. H., *J. Phys. Chem. B.* **103**, 4611 (1999).
74. Volodin, A. M., Sobolev, V. I., and Zhidomirov, G. M., *Kinet. Catal.* **39**, 775 (1998).
75. Abragam, A., and Bleany, B., "Electron Paramagnetic Resonance of Transition Ions." Oxford Univ. Press, London, 1970.
76. Pilbrow, J. R., "Transition Ion Electron Paramagnetic Resonance." Oxford Univ. Press, New York, 1990.
77. Joyner, R., and Stockenhuber, M., *J. Phys. Chem. B.* **103**, 5963 (1999).
78. Kucherov, A. V., Montreuil, C. N., Kucherova, T. N., and Shelef, M., *Catal. Lett.* **56**, 173 (1998).
79. Battiston, A. A., Bitter, J. H., and Koningsberger, D. C., *Catal. Lett.* **66**, 75 (2000).